

Cit this: *JOWSET*, 2018 (03), N°01, 305-314

The removal and desorption of two toxic dyes from aqueous solution by hydroxylated hematite sand: Kinetics and equilibrium

M. Abbaz*, Y. Azougarh, M. Benafqir, R. El Haouti, S. Lhanafi and N. El Alem

Materials and Environment Laboratory (MEL), Department of Chemistry, Faculty of Science, Ibn Zohr University, city Dakhla B.P 8106, Agadir – Morocco

*Corresponding author, E-mail: abbaz.2203@gmail.com; nelalem@gmail.com, Tel: +212641388265; Fix: +212528242217

The adsorption/desorption properties of hematite sand (HS) for removal of two toxic dyes have been tested in aqueous solution by batch process. The raw sand and HS were characterized. Toluidine blue (TB) and crystal violet (CV) were selected as a toxicity model. The effect of adsorbent dose, contact time, pH solution and ionic strength was investigated. The dye adsorption was influenced significantly by the presence of inorganic salt (KCl). The best fitted equilibrium and kinetic model for two dyes were found to be Langmuir and pseudo-second order, respectively. Intra-particle diffusion is not the only speed-controlled step. The maximum monolayers capacities of TB and CV were 1.60×10^{-5} and 2.65×10^{-5} mol.g⁻¹, respectively with the optimal equilibrium time of 60 min at room temperature and pH 10. In the batch desorption process, 0.2 M NH₄Cl achieved better performance for both dyes desorption and the HS can be effectively reused for four cycles consecutively.

Received: 17 June 2017
Accepted: 24 March 2018
Available online: March 2018

Keywords:

Hematite sand
Adsorption/desorption
Toxic dye

1. Introduction

A wide range of dyes, due to their dyeing properties, are primarily used in the textile industry for colouring various materials, such as leather, plastics, paper, food and petroleum products. Some dyes and their by-products may be carcinogens and toxics and can cause damage not only to aquatic life but also to human beings. Cationic dyes are a more toxic, carcinogenic and mutagenic than anionic dyes due to their synthetic origin and aromatic ring structure with delocalised electrons [1].

The toluidine blue and crystal violet, two well-known cationic dyes, have been widely used for different purposes in several fields. Toluidine blue is an acidophilic metachromatic dye that selectively stains acidic tissue components [2]. Toxicological studies indicate that TB can significantly decrease the mean

half-life of motile bull spermatozoa [3] and has a mutagenic potential [4]. Crystal violet, a typical tri-phenyl methane dye, is widely applied in the textile industry. It is poorly degraded as recalcitrant molecule by microbial enzymes, and can persist in a variety of environments [5]. Several biological, physical, chemical and discoloration methods have been reported to tackle the removal of dyes from aqueous solution [6]. Literature data reveals that solid/liquid separation method by adsorption is one of the most popular methods for the removal of pollutants from wastewater. Different natural materials, which includes bentonite, siliceous sand, clays, Gypsum etc. [6-9] have been tested for cationic dyes adsorption from aqueous solutions. In addition, several studies have been done to test carbon materials [10-12] but they are expensive and the cost of regeneration is high because desorption of the dye molecules is not easily achieved [13].

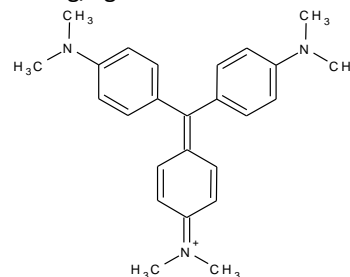
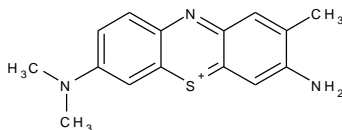
The aim of the present research is to test the adsorptive properties of hematite sand (HS) as a new adsorbent for removing toluidine blue (TB) and crystal violet (CV) in aqueous solutions. Also, we attempt to optimize desorption process by using different desorbing agents. Four cycles of adsorption/desorption were performed to study the reliability of HS. This study is novel as no literature citations are available where HS has been used for removing toxic dyes from aqueous solution.

2. Materials and methods

Tab 1: The physical and chemical characteristics of toluidine blue and crystal violet dyes

Physical and chemical properties	Toluidine blue	Crystal violet
Color index number	52040	42555
Generic name	Basic blue 17	Basic Violet 3
Molecular formula	C ₁₅ H ₁₆ N ₃ SCl	C ₂₅ H ₃₀ N ₃ Cl
Molecular weight (g/mol)	305.8	407.98
Max absorbance λ_{max} (nm)	635	589–594 nm
Solubility in water	50 g/l (20°C)	16 g/l (25 °C)
Natural pH value (20 mg/l water)	4.8 - 5.2	5.5 – 6.2
Toxicity LD50 (Rat)	250 mg/Kg	420 mg/Kg

Structure



2.2 Preparation of HS and characterisation

The raw sand was collected in Taghazout beach (North-East of Agadir, Morocco). The collected material was repeatedly washed with distilled water to remove all earthen impurities and then dried in an oven at 30°C for 24 h. After drying, the sample was sieved to obtain desired particle sizes (80 – 100 μm). Then, it was oxidised for 20 min at 60 °C in a 1/1/5 mixture of 25 % NH₄OH, 30 % H₂O₂ and H₂O. After the reaction, the material was washed with distilled water until the pH reaches neutral followed by acetone. Finally, the sample was dried in an Airstream at 30 °C and stored in a desiccator until used as hematite sand (HS).

The raw sand and HS were characterised by X-ray diffraction (Phillips X'pert Pro spectrometer, Cu-K α , $\lambda = 0.1548$ nm). Identification of the minerals contained in the sample was achieved by comparing the X-ray pattern with a database (Joint Committee on Powder Diffraction Standards-International Center for Diffraction Data). The Fourier

2.1 Materials and Reagents

The toluidine blue and crystal violet dyes were purchased from Sigma–Aldrich and used without purification. An accurately weighed quantity of dye was dissolved in 1L of double-distilled water to prepare a stock solution (100 mg.L⁻¹). Experimental solutions of the desired concentrations were obtained by successive dilutions. The characteristics and chemical structure of the dye are listed in Tab. 1. KCl, KOH and NH₄Cl were purchased from Fluka and KNO₃ was purchased from Sigma–Aldrich. All the chemical reagents are of analytical grade and used without further purification.

Transform infrared spectrums (FTIR) were performed by VERTEX 70 spectrometer in the range 400 – 4000 cm⁻¹ with a resolution of 4 cm⁻¹ using KBr pellets to elucidate the functional groups present on the surface of raw sand and HS. The textural characterisation (surface area and total pore volume) of HS was carried out by N₂ adsorption-desorption isotherms at 77 K (Quantachrome Autosorb). X-ray fluorescence (XRF, Axios PW4400) was used to determine the main component present in the HS particles. According to [14; 15] the surface charge density σ (C.m⁻²) can be calculated as:

$$\sigma = \frac{Q \times F}{S_{\text{BET}}} \quad (1)$$

Where, Q (mol.g⁻¹) is the mean surface charge, F (96,500 C.mol⁻¹) is Faraday's constant and S (m².g⁻¹) is the surface area. Q can be calculated as a function of pH from the difference between the concentration of added base or acid and the equilibrium concentrations of HO⁻ and H⁺ for a given amount of adsorbent in 0.01 M KCl.

2.3 Adsorption experiments

Batch adsorption studies were carried out by contacting a known amount of HS with 25 mL of dye solution of known initial dye concentration in 30 mL stoppered conical flask. This mixture was agitated in a temperature controlled shaking water bath at a constant speed of 100 rpm. The effect of the adsorbent amount (by varying it in the range of 0.2 – 5.0 g) and the contact time were studied with the initial dye concentration of 20 mg.L⁻¹ at 25 °C. Effect of pH on dye removal was studied over a pH range of 3 – 11. The initial pH of the solution was adjusted by addition of dilute aqueous solutions of HCl or KOH (0.1 M). KCl was added to adjust the background ionic strength to 0.01 M. The effect of ionic strength on the removal efficiency of dye onto adsorbent was discussed over the KCl concentration range from 0.0 to 1 mol.L⁻¹. The adsorption isotherm was carried out at different initial concentration of dye under optimal pH condition at 25 ± 1 °C. The contact was made for 5 h, which is more than sufficient time (predetermined) to reach equilibrium. After, the dye solutions were separated from the adsorbent by syringe filter (0.45 µm pore size, Whatman). At the end of adsorption experiments, the dye concentration was determined at λ_{max}, using UV spectrophotometer (Jenway Model 6800) and then applying Beer–Lambert law. The adsorption capacity was calculated using the following equation:

$$q = \frac{(C_0 - C_e)}{m} \times V \quad (2)$$

Where C₀ and C_e are initial and equilibrium concentrations of TB (mol.L⁻¹), respectively, V is the volume of the solution (L) and m is the weight of adsorbent (g). The percentage removal of dye was calculated using the following relationship

$$\% \text{ dye removal} = \frac{(C_0 - C_e)}{C_0} \times 100 \quad (3)$$

2.4 Desorption process

Batch process was used for desorption studies in which known amount of adsorbent was taken in 25 ml of dye solution (20 mg.L⁻¹) at 25°C. After adsorption the solution was filtered and adsorbent was washed with distilled water to remove any excess of dye solution. Desorption studies were conducted using different desorbing agents like HCl, NH₄Cl, KNO₃, KCl and deionized water. The HS adsorbent loaded with dye was placed in the desorbing medium (10 mL) and was constantly stirred on a rotatory shaker at 100 rpm for two hours at 23 ± 1°C. Then the supernatant solutions were analysed by UV–vis spectrometry. Desorption efficiency (%) was estimated from the following standard equation:

$$\% \text{ Desorption} = \frac{C_d}{C_a} \times 100 \quad (4)$$

Where C_d and C_a are the concentration of dye (mol.L⁻¹) desorbed and adsorbed, respectively. After regeneration, the adsorbent was again used for the further adsorption of dye. The adsorption and desorption experiments were repeated for four cycles.

2.5 Mathematical modelling

2.5.1 Isotherm modelling

The non-linear forms of the Langmuir and Freundlich isotherm models [16] were used to analyse the equilibrium isotherm data. The parameters, which were obtained from different models, provided important information to the adsorption mechanisms, surface properties and affinities of the adsorbent [17]. The Langmuir model [18] assumes monolayer coverage of adsorbate over a homogenous adsorbent surface and that the adsorption of each molecule onto the surface has the same activation energy of adsorption. The Langmuir isotherm model can be represented by the following equation:

$$q_e = \frac{q_m K_L C_e}{1 + K_L C_e} \quad (5)$$

Where q_m (mol.g⁻¹), is the maximum adsorption capacity amount of dye at complete monolayer coverage, and K_L (L.mol⁻¹) is the constant related to the heat of adsorption. The Freundlich isotherm [19] is an empirical equation which assumes that the adsorption occurs on heterogeneous surfaces. The Freundlich equation can be expressed as:

$$q_e = K_F C_e^{1/n} \quad (6)$$

Where, K_F (mol.g⁻¹) and 1/n are Freundlich constants. The constant K_F is related to degree of adsorption, n provides the rough estimation of the intensity of the adsorption.

A trial-and-error procedure was used for the non-linear method using the solver add-in with Microsoft Excel, 2010 [20]. The non-linear Chi-square test statistic χ² (Eq. 7) and the correlation coefficient R² (Eq. 8) were used to estimate various isotherm parameters and establish the best correlation to explain experimental data [16; 20]. The best fit model was selected by the highest R² and lowest χ².

$$\chi^2 = \sum_{i=1}^P \left[\frac{(Q_{\text{exp}} - Q_{\text{mod}})^2}{Q_{\text{mod}}} \right] \quad (7)$$

$$R^2 = \frac{\sum (Q_{\text{exp}} - \overline{Q_{\text{mod}}})^2}{\sum (Q_{\text{exp}} - \overline{Q_{\text{mod}}})^2 + \sum (Q_{\text{exp}} - Q_{\text{mod}})^2} \quad (8)$$

Where Q_{exp} and Q_{mod} are the amount of MB adsorbed at equilibrium from experiments and from models, respectively and $\overline{Q_{\text{mod}}}$ is the average of Q_{mod}.

2.5.2 Kinetic models

In order to investigate the mechanism of adsorption, two kinetic models, namely, pseudo-first order of Lagergren and pseudo-second order equations were analysed. The Lagergren rate equation is one of the most widely used adsorption rate equations for the adsorption of the solute from a liquid solution. The linearized integral form of the pseudo-first-order model generally expressed as:

$$\ln(q_e - q_t) = \ln q_e - K_1 t \quad (9)$$

Where q_e is the amount of adsorbed dye at equilibrium time and K_1 (min^{-1}) is the rate constant of the pseudo-first order model. In this model, the plot of $\ln(q_e - q_t)$ versus t should give a linear relationship from which K_1 and q_e can be determined from the slope and the intercept of the resulted plot, respectively. It is reported by [21], [22] and [23] that in many cases the above equation does not fully describe the adsorption kinetics. In such cases, a pseudo-second order equation can be used, which is given by the following equation:

$$\frac{t}{q_t} = \frac{1}{K_2 \times q_e^2} + \frac{t}{q_e} \quad (10)$$

Where K_2 ($\text{g} \cdot \text{mol}^{-1} \cdot \text{min}^{-1}$) is the rate constant of the pseudo-second order model. The parameters K_2 and q_e can be obtained from the plot of (t/q_t) versus t that should show a linear relationship. To further evaluate the controlling step of the adsorption process of both dyes onto HS, we used the intra-

particle diffusion model according to the method reported by Weber and Morris. This model can be expressed by the following equation:

$$q_t = K_{\text{ind}} t^{0.5} + C \quad (11)$$

Where K_{ind} ($\text{mol} \cdot \text{min}^{-0.5} \cdot \text{g}^{-1}$) is the rate constant of the intra-particle diffusion and C is the boundary layer thickness ($\text{mol} \cdot \text{g}^{-1}$). It is clear that the plot of q_t vs. $t^{0.5}$ should be linear according to (Eq. 10). If a plot of q_t vs. $t^{0.5}$ gave a straight line, the adsorption process should involve the intra-particle diffusion [24; 25] and if this line passed through the origin, the particle diffusion would be the controlling step.

3. Results and discussion

3.1 Characterization of HS

As a comparison, the XRD patterns of raw sand and HS were shown in Fig. 1a. The diffractogram of raw sand before treatment displays six main diffraction peaks at $2\theta = 24.20^\circ$, 33.12° , 35.59° , 40.89° , 49.53° and 54.10° that can be assigned to hematite Fe_2O_3 (JCPDS card, file No. 24-0072). Other peaks are also observed at $2\theta = 20.87^\circ$, 26.28° and 50.65° , at $2\theta = 20.87^\circ$, 26.28° and 50.65° which may be related to the presence of quartz SiO_2 (JCPDS card, file No. 46-1045) and rutile TiO_2 (JCPDS card, file No. 76-0335), respectively. After treatment, the peaks at 20.87° , 29.43° and 45.78° belonging to silicate and calcite disappeared from the system, and hematite Fe_2O_3 is still the major phases on the grain surface.

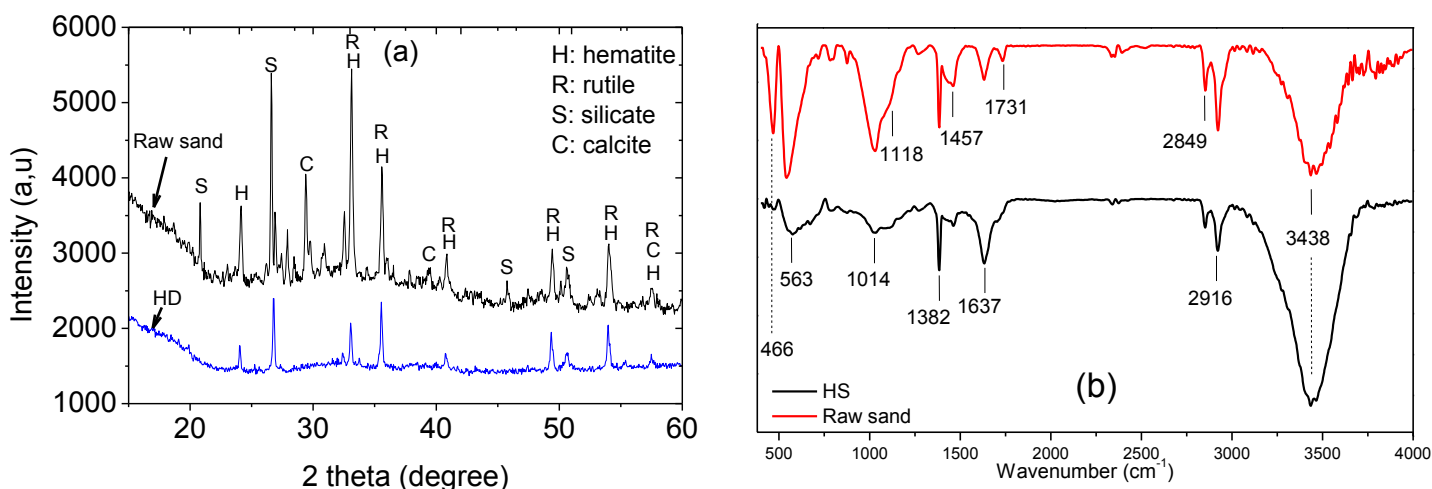


Fig. 1: X-ray diffraction (a) and FTIR spectrums (b) results obtained for raw sand and HS.

The presence of functional groups on the surface of both materials was confirmed by using FTIR analysis (Fig. 1b). An intense and broad band appeared in the $3200 - 3600 \text{ cm}^{-1}$ region and the band centred in 1632 cm^{-1} indicating the presence of free or hydrogen-bonded $-\text{OH}$ groups. This, gives

the existence of $\text{Ti}-\text{OH}$ at 3667 cm^{-1} [26; 27], $\text{Fe}-\text{OH}$ groups or $\text{Zr}-\text{OH}$ at 3400 cm^{-1} [28] including 3681 and 800 cm^{-1} which were due to $\text{Si}-\text{OH}$ [7]. The relatively high intensity of hydroxyl groups peaks suggested that large number of hydroxyl groups were present in the surface of HS. These groups may function as

proton donors hence, deprotonated hydroxyl groups may be involved in coordination with dyes. Three major peaks were detected at 466, 542 and 1030 cm^{-1} in the raw sand which corresponds to the binding vibration of Si-O groups [29; 30]. Whereas in the case of HS, no vibration band at 466 cm^{-1} indicates that treated HS have less number of Si-O groups on its surface.

Fig. 2 shows the surface charge density of raw sand and HS as a function of pH. The surface charge density can be seen to decrease as the pH is raised and the intersection of the curve with the x-axis gives the zero point of charge (pH_{ZPC}). The pH_{ZPC} of raw sand and HS is found to be 5.40 and 6.20 respectively as illustrated in Fig. 2. The pH_{ZPC} of HS was influenced by the chemical composition of the grain surface, mainly composed of hydroxyl groups. At $\text{pH} < \text{pH}_{\text{ZPC}}$, the surface of both materials has a net positive charge, while at $\text{pH} > \text{pH}_{\text{ZPC}}$ the surface has a net negative charge [31].

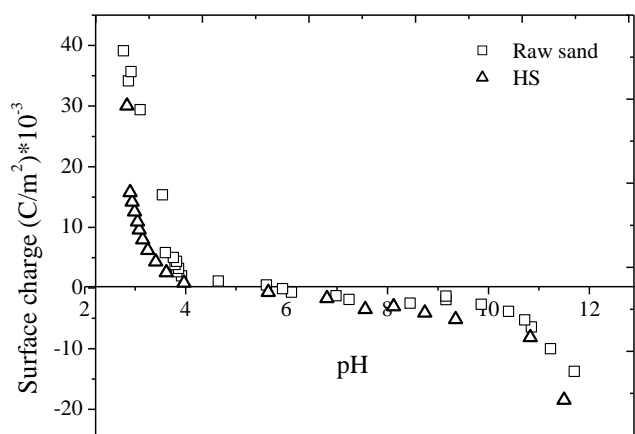


Fig. 2: Surface charge with different pHs for raw sand and HS in 0.01 M KCl.

The chemical composition of HS determined by X-ray fluorescence spectrometer is Fe_2O_3 , 84.4; TiO_2 , 8.1; SiO_2 , 2.79; ZrO_2 , 5.15; Al_2O_3 , 0.57; CaO , 0.51; MgO , 0.338; SO_3 , 0.15; K_2O , 0.13; and Na_2O , 0.15 and lost in ignition, 0.51 wt%. The particle size distribution was found between 3.6 and 181 μm (determined by the method of a laser beam dispersion using the Malvern 2000 particle size analyser). The specific surface area, total pore volume and average pore diameter obtained from the N_2 equilibrium adsorption isotherms were found to be 0.84 m^2g^{-1} , 0.0132 cm^3g^{-1} and 2.64 nm, respectively. This value is relatively smaller than other previously reported in the literature [32] for sand materials but is expected to be enough for enhancing the adsorption of two toxic dyes.

3.2 Adsorption of CV and TB

3.2.1 Optimization of adsorbent dosage and effect of contact time

The effect of adsorbent dosage and contact time for the adsorption of CV and TB on HS was studied for a period of 5 h for initial dye concentration of 20 $\text{mg}\cdot\text{L}^{-1}$ at room temperature and natural pH, as depicted in Fig. 3.

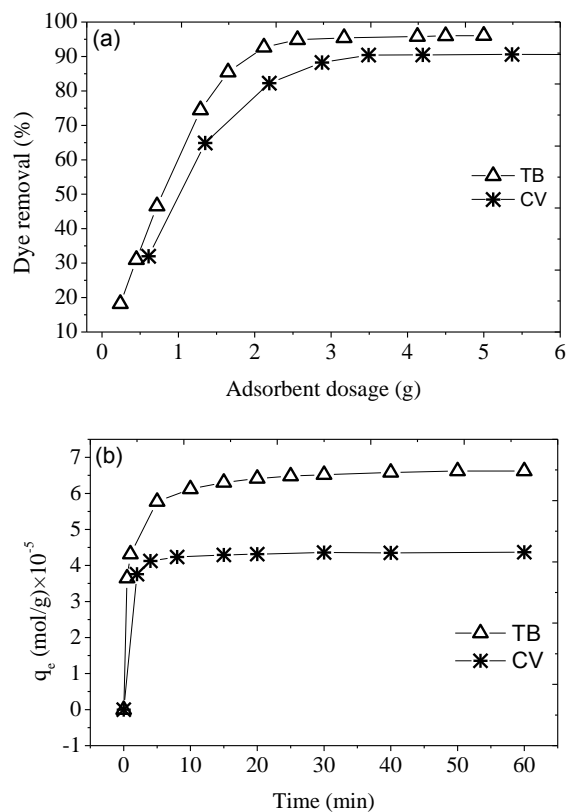


Fig.3: Effect of adsorbent dosage (a) and contact time (b) on the adsorption of TB and CV by HS.

From the Fig. 3a it has been found that adsorption of both dyes increases with adsorbent dose and attained a constant value when equilibrium was established. The optimum amount of HS was found to be 2.5 g for TB and 3.5 for CV, which was used for all further adsorption studies. The increase in the percentage of dye removal with adsorbent dosage could be attributed to an increase in the adsorbent surface area, augmenting the number of hydroxyl groups available for adsorption. Fig. 3b represents the adsorption capacity versus the adsorption time. The number of both dyes adsorbed increased with increase in contact time and reached equilibrium after 40 min. After this time, no obvious variation in dye adsorbed was examined. Based on these results, 60 min was taken as the equilibrium time in batch adsorption experiments.

3.2.2 Effect of pH and ionic strength

The pH and ionic strength of salts affect the degree of ionisation of dye molecular, the surface properties and the modification of functional groups on the active sites of the adsorbent [33]. Fig. 4a clearly displays the pH dependency on TB and CV adsorption efficiency onto HS. As shown, the removal rates

increased from 89.47 % to 98 % for both dyes as the pH was increased from 3 to 11. A large increase in the removal rate for both cationic dyes was observed under basic conditions and occurs in a wide range of pH (5 -11). This can be explained in terms of pH_{ZPC} . The pH_{ZPC} of the HS is about 5.40 as observed from the Fig. 2. At pH values lower than the pH_{ZPC} , the surface of the adsorbent is positively charged. Thus, a decrease in the removal of dye is apparently due to the higher concentration of H^+ ions that are competing with the positively charged dyes for adsorption sites (OH groups) of HS. Moreover, as the pH of the dye solution becomes higher ($pH > pH_{ZPC}$), the number of the negatively ionisable sites on the grain surface increases, facilitating the adsorption of cationic dye [34]. The increase in the amount of adsorbed dye when increasing the pH value suggests that the electrostatic interactions between the OH present in HS and the positively charged cationic dyes contribute to the adsorption process. It should also be noted that the constant removal rate for CV over the pH ranges 5.5 – 7.5 is an indication that the electrostatic mechanism was not the only mechanism for dye adsorption in this system. HS can also interact with dye molecules via hydrogen bonding.

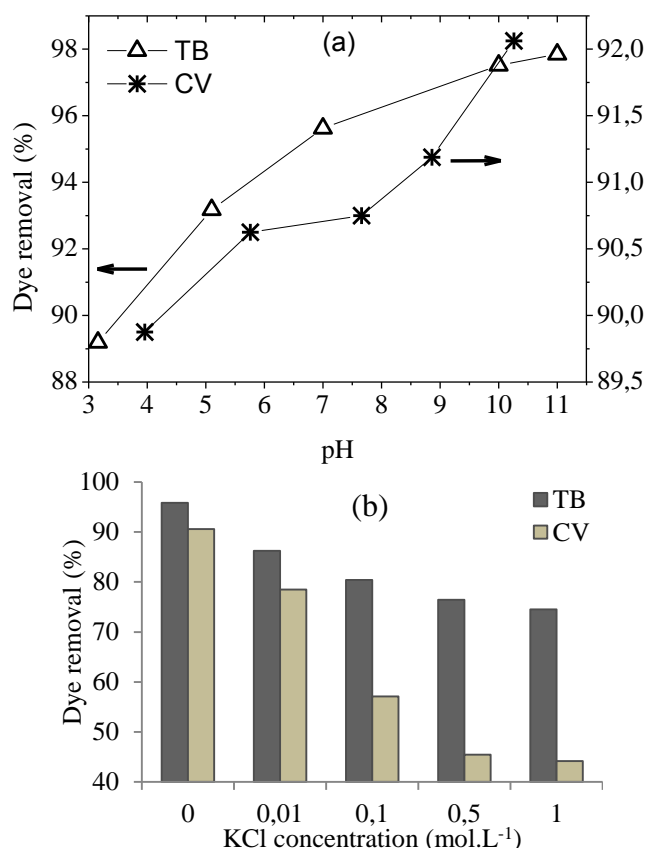


Fig. 4: Effect of initial solution pH (a) and ionic strength (b) on the adsorption of TB and CV.

In order to further explore whether electrostatic interactions controlled the adsorption process or not, the effect of ionic strength on adsorption of the two dyes onto the HS was

investigated. The effect of ionic strength (Fig. 4b) was tested by the addition of different concentrations of KCl (0 – 1 mol/L) to initial dye solution of 20 mg.L⁻¹ at natural pH (5 - 6). As seen in Fig. 4b, the removal percentage of dye decreases significantly with the increase in the salt concentration. This behaviour could be attributed to the competition between cationic dye and K^+ ion for the active adsorption sites [35]; [36]. Indeed, the salt can screen the electrostatic interaction between the group hydroxyls and the dye molecules, and makes the adsorption capacity for dye decrease with increasing KCl concentration. A large decrease in the removal rate for CV dye was observed at 0.5 M. The obtained results gave an indication that this adsorption process for CV is mainly governed by the electrostatic attractions.

A proposed mechanism [5; 35; 37] for the adsorption of CV and TB onto the HS material is shown in Fig. 5.

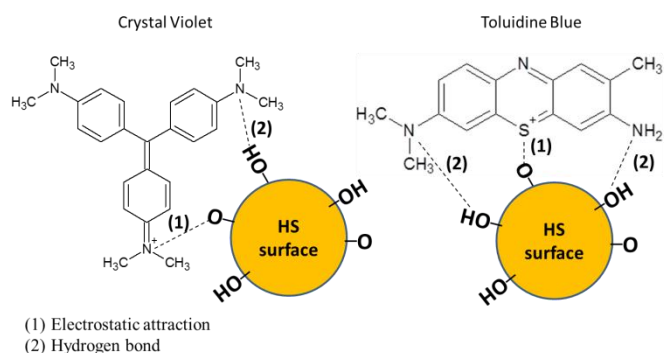


Fig. 5: Schematic representation of hydrogen bonding and electrostatic attraction between dye molecules and hydroxyl groups on the HS surface

3.2.3 Adsorption isotherm

In order to appreciate the interaction between the adsorbate and adsorbent, adsorption isotherm data starting at different initial dye concentrations were investigated to fit the models of Langmuir and Freundlich. Fig. 6 depicts the amounts of TB and CV adsorbed by HS against the equilibrium concentrations at ambient temperature (25 ± 1 °C). The best-fit values of the model parameters estimated from Eqs. (5) and (6) by non-linear regression analyses are listed in Tab 2. According to Giles's classification [38], the isotherms are of L-type, indicating that two dyes have a high affinity for HS and there is no strong competition of the solvent (water) for the active sites of adsorption. As can be seen (Tab. 2), the Langmuir isotherm exhibited the best fit with the experimental equilibrium data due to its higher R^2 (≥ 0.97) and lower χ^2 values (≤ 0.001) compared to the Freundlich. The Langmuir model assumes that adsorption occurs on a surface which is composed of a fixed number of binding sites of equal energy, one molecule being adsorbed per binding site with no interaction between adsorbed molecules until monolayer coverage is achieved. The maximum monolayer adsorption was 1.60×10^{-5} and 2.65×10^{-5}

mol/g for TB and CV, respectively. Furthermore, K_L indicates the affinity of the dye to bind with the adsorbents. A high K_L value indicates a higher affinity [39]. Based on these values, CV had higher adsorption affinity for HS compared to TB. The difference in binding affinity may be attributed to the difference in the number of functional groups carried by the two dyes. In the Freundlich isotherm, the constant $1/n$ is a measure of exchange intensity or surface heterogeneity, with values between 0 and 1. In this study, the values of n were more than 1 (Tab. 2). This suggested that the adsorption conditions were favourable. High values of $1/n$ indicate a strong bond between the substrate and the dye.

The values of maximum adsorption capacity of cationic dyes calculated from Langmuir equation are compared with other low-cost adsorbents in the literature and summarised in Tab. 3. From these values, HS is better or comparable to other reported adsorbents for the removal of CV and TB.

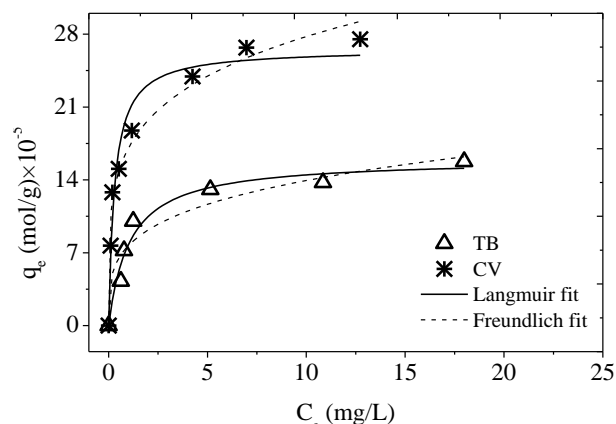


Fig.6: Adsorption isotherms of TB and CV by HS from aqueous solution. Curves represent the non-linear fitting of the experimental data to the Langmuir and Freundlich equations.

Tab 2: Langmuir and Freundlich parameters for two dyes adsorption by treated HS

	Langmuir isotherm				Freundlich isotherm				q_e (exp.) (mol.g ⁻¹)
	q_m (mol.g ⁻¹)	K_L (L.g ⁻¹)	R^2	χ^2	K_F (mol.g ⁻¹)	$1/n$	R^2	χ^2	
TB	1.60×10^{-5}	0.94	0.978	0.00100	0.768×10^{-5}	0.258	0.963	0.0020	1.54×10^{-5}
CV	2.65×10^{-5}	3.36	0.983	0.00014	1.70×10^{-5}	0.226	0.975	0.0002	2.78×10^{-5}

Tab 3: Comparison for the removal of TB and CV dyes at room temperature (25 – 30 °C) by different low-cost adsorbents

Dye	adsorbent	S_{BET} (m ² g ⁻¹)	Maximum adsorption capacity (mol/g) × 10 ⁻⁶	Reference
TB	Fly ash	7.1	84.96	[40]
	Gypsum	5.67	68.62	[21]
	kraft fibers	-	31.04	[36]
	Hematite sand (HS)	0.84	16.0	This work
CV	nanomagnetic iron oxide	-	31.12	[41]
	magnetic zeolite (MZ)	-	2.37	[42]
	Magnetically modified spent grain	-	98.52	[43]
	Bottom ash	-	24.0	[44]
	De-oiled soya	-	30.88	[44]
	MWCNTs/Mn _{0.82} Ni _{0.2} Fe ₂ O ₄ composite	59.8	12.25	[45]
	Date palm fibers (DPFs)	-	1.61	[46]
	Orange peel	20	28.18	[47]
	Peat	-	20	[48]
	Hematite Sand (HS)	0.84	26.5	This work

3.2.4 Kinetic studies

To elucidate the adsorption kinetic process, the results of Fig. 3b were fitted using pseudo-first order, pseudo-second order, and intra-particle diffusion (Fig. 7 and Fig. 8). The parameters and linear correlation coefficients calculated from the slope and

intercept of fitting plots are listed in Tab. 4. The correlation coefficient ($R^2 \geq 0.99$) values for the second-order kinetic model were higher than Lagergren kinetic. The calculated q_e values also agree very well with the experimental data. These results indicate that the adsorption system studied belongs to the

second-order kinetic model. This implies that the adsorption might be governed by chemisorption which involved the formation of covalent bonds between dye molecules and the adsorbent [34]. A chemisorption mechanism only allows for a monolayer adsorption [49], which is in good agreement with Langmuir model that best describes the equilibrium adsorption data.

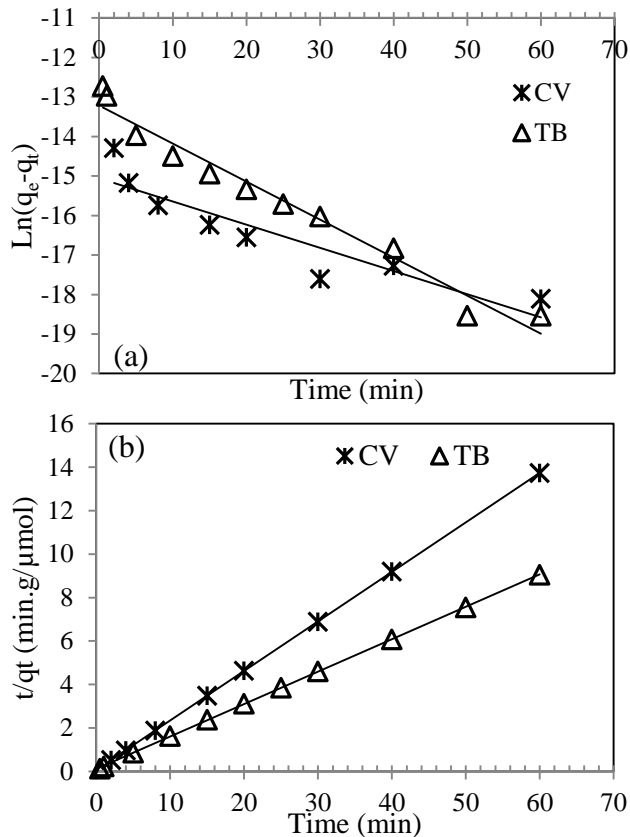


Fig. 7: Pseudo-first order (a) and Pseudo-second order (b) plots for the removal of TB and CV from aqueous solution by HS

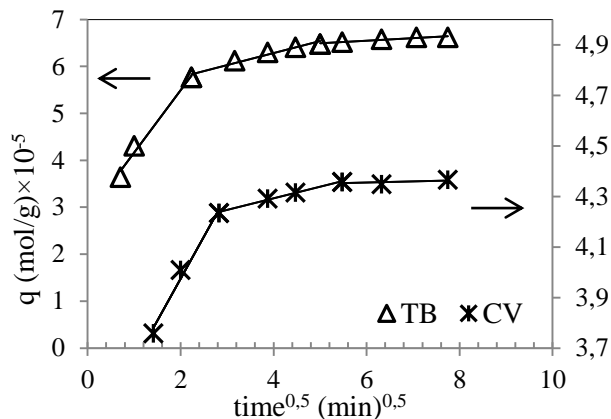


Fig.8: Weber and Morris intra-particle diffusion plot for the removal of TB and CV by HS.

The intra-particle diffusion kinetic for adsorption of both dyes onto treated HS is shown in Fig. 8. The plots (q_t versus $t^{1/2}$) present multi-linearity and do not pass through the origin, which indicates that the intra-particle diffusion is not the only rate controlling step but also other kinetic models may control the rate of adsorption. The first linear portion was attributed to the fast mass transfer of dye molecules from aqueous solution to the external adsorbent surface or boundary layer diffusion of solute molecules. The second linear portion is the gradual equilibrium stage with intra-particle diffusion dominating. The third portion is attributed to the final equilibrium stage for which the intra-particle diffusion starts to slow down due to the extremely low adsorbate concentration left in the solution. Extrapolation of the linear portions of the plots back to the y-axis gives the intercepts, i.e. the value of C, which provides the measure of the boundary layer thickness. If the intercept is large, the boundary layer effect will also be large

Tab 4: Kinetic parameters calculated from Pseudo-first order, Pseudo-second-order model and Weber-Morris kinetic models for TB and CV adsorption.

	Pseudo-first-order model			Pseudo-second-order model					
	K_1 (min^{-1})	Q_e ($\text{mol/g}) \times 10^{-6}$	R^2	K_2 ($\text{g.mg}^{-1}\text{min}^{-1}$)	Q_e ($\text{mol/g}) \times 10^{-6}$	R^2			
TB	0.096	1.82	0.967	0.200	0.6697	0,999			
CV	0.058	2.87	0.835	0.757	4.3800	1			
Weber-Morris kinetic model									
	Initial linear portion			Second linear portion			Third linear portion		
	K_d ($\text{mol/g.min}^{1/2}$)	C	R^2	K_d ($\text{mol/g.min}^{1/2}$)	C	R^2	K_d ($\text{mol/g.min}^{1/2}$)	C	R^2
TB	1.32	2.83	0.983	0.2550	5.26	0.959	0.0540	6.223	0.930
CV	0.33	3.31	0.983	0.0460	4.12	0.993	0.0048	4.326	0.834

3.3 Desorption and regeneration studies

Desorption–adsorption experiments have also been performed in a batch mode to evaluate the possibility of regeneration and reuse of the adsorbents for removal of cationic dyes. Selection of an appropriate eluent is crucial for successful regeneration.

Five different desorbing agents as eluents (Fig. 9) were tested in order to find a suitable desorbent for dye recovery from HS. As illustrated in Fig 9, solutions of salt (KNO_3 , KCl , and NH_4Cl) were very efficient (desorption yield in the range of 30 – 80 %). The other eluents (Deionised water, HCl), shows a much lower capability for both dyes desorption in the range of 1-10 %. A maximum desorption percentage using 0.1 M NH_4Cl solution was found to be about 82 % and 64 % for TB and CV, respectively. Thus, NH_4Cl was chosen as a desorbing agent for further desorption studies. Inefficient desorption in hydrochloric acid indicates that CV was strongly attached onto bottom ash through chemisorption. Similar results were observed for the adsorption of CV by treated ginger waste [50]. Influence of NH_4Cl concentration on desorption of both dyes from dye-saturated HS was presented in Fig. 10. It can be observed that the maximum desorption of dye (92 % for TB and 78 % for CV) could be reached using 0.2 M NH_4Cl solution. We observe a decrease of desorption of CV at higher concentrations of NH_4Cl . The high desorption in salt medium indeed reveals that the adsorption of TB and CV onto the HS is mainly controlled by electrostatic attraction, which is consistent with the results obtained previously.

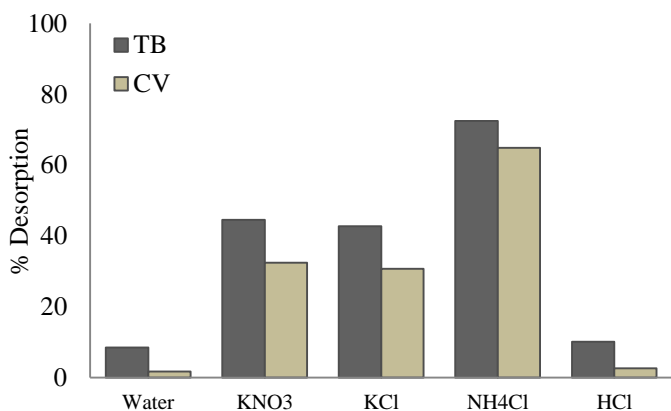


Fig. 9: TB and CV desorption from HS using various eluents for 1h (Deionised Water, 0.1 M KNO_3 , 0.1 M KCl , 0.1 M NH_4Cl and 0.01M HCl).

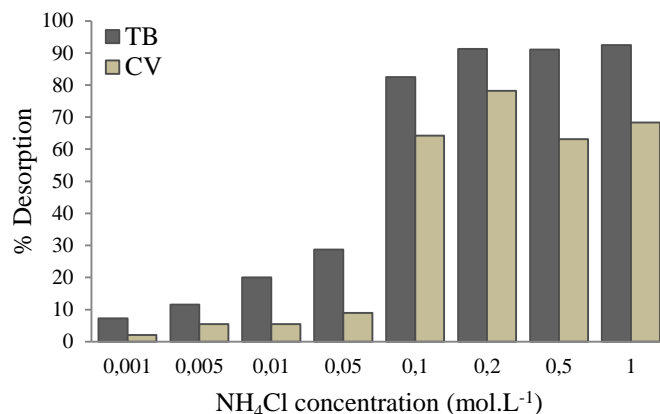


Fig. 10: Influence of NH_4Cl concentration on desorption of TB and CV from HS for two hours at $23 \pm 1^\circ\text{C}$.

Regeneration of HS is an important step in order to check the economic feasibility of adsorption process. The regeneration studies were carried out in batch mode for four successive cycles (Fig. 11) using 0.2 M NH_4Cl for both dyes, since this solution exhibited the highest desorption performance (Fig. 10). As shown in Fig. 11, HS could be regenerated and reused for up to three or more adsorption/desorption cycles.

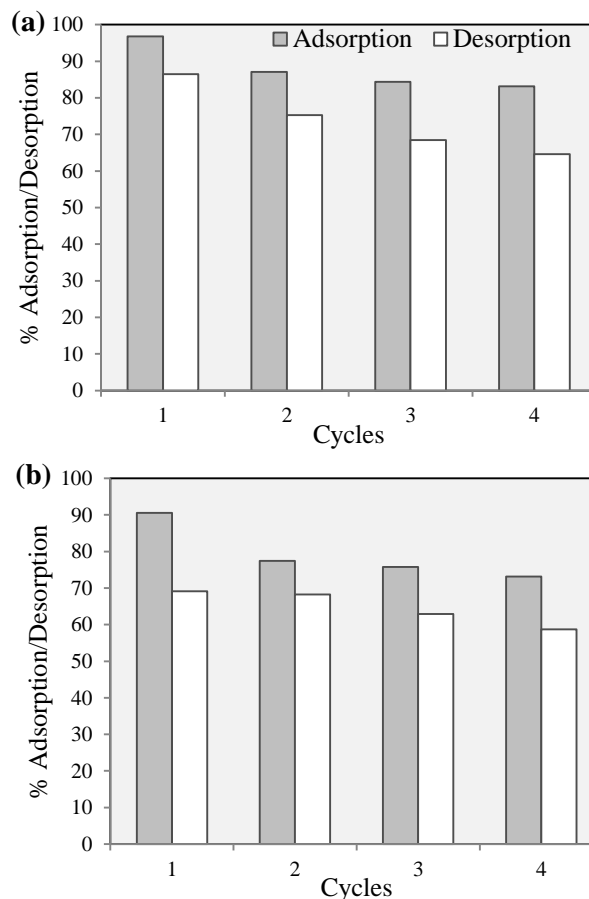


Fig.11: Regeneration process of HS for four adsorption /desorption cycles of (a) TB and (b) CV with 0.2 M NH_4Cl solution.

Conclusion

This investigation shows that hematite sand (HS) can be successfully used for the adsorption of TB and CV as two toxic dyes from aqueous solution. Batch adsorption experiments show that the adsorption of two dyes onto HS was dependent on many variables including adsorbent dosage, time, pH, ionic strength, concentration of the dye. The removal of both dyes increased with increase in pH from 3 to 11, with the maximum removal (> 98 %) at pH 11. It was found that the dye adsorption decreased in the presence of KCl. The hydrogen-bonding interaction, electrostatic attraction and chemical association are the main driving force for the adsorption process. The adsorption isotherm data were fitted to Langmuir and Freundlich equations by non-linear regression method. The equilibrium data fitted better with the Langmuir isotherm equation and the maximum monolayers capacities of TB and CV were 1.60×10^{-5} and 2.65×10^{-5} mol.g⁻¹, respectively. The equilibrium dye/adsorbent was practically achieved in 60 min and adsorption kinetics was found to follow a second-order rate expression. HS can be easily regenerated using 0.2 M NH₄Cl and applied for four frequent sorption/desorption cycles with high performance. Finally, HS presents great potential as an inexpensive and easily available alternative adsorbent for the removal of toxic dyes.

Acknowledgments

We wish to thank the LME laboratory team at Ibn Zohr University for financial support. Authors also acknowledge Moroccan Foundation for Advanced Science, Innovation and Research (MAScIR) for extending N₂ adsorption-desorption analysis of the samples. We would like to thank the reviewers for their time spent on reviewing our manuscript and their comments.

References

1. A Appusamy, I John, K Ponnusamy, and A Ramalingam, *Eng. Sci. Technol. an Int. J.*, **2014**, 17, 137.
2. M. A. Kuriakose, *Contemporary Oral Oncology: Biology, Epidemiology, Etiology, and Prevention*. **2016**.
3. C. van Duijn, *Exp. Cell Res.*, **1962**, 26, 373.
4. A. J. Dunipace, R Beaven, T Noblitt, L Yiming, S Zunt, and G Stookey, *Mutat. Res. Toxicol.*, **1992**, 279, 255.
5. Y Lin, X He, G Han, Q Tian, and W Hu, *J. Environ. Sci.*, **2011**, 23, 2055.
6. M. A. Rauf, S. M. Qadri, S Ashraf, and K. M. Al-Mansoori, *Chem. Eng. J.*, **2009**, 150, 90.
7. K Mukherjee *et al.*, *RSC Adv.*, **2015**, 5, 30654.
8. R Sahraei, *RSC Adv.*, **2016**, 6, 72487.
9. G Rytwo, S Nir, M Crespian, and L Margulies, *J. Colloid Interface Sci.*, **2000**, 222, 12.
10. B. H. Hameed, A. L. Ahmad, and K. N. A. Latiff, *Dye. Pigment.*, **2007**, 75, 143.
11. H Yu and B Fugetsu, *J. Hazard. Mater.*, **2010**, 177, 138.
12. N. A. Travlou, G. Z. Kyzas, N. K. Lazaridis, and E. A. Deliyanni, *Langmuir*, **2013**, 29, 1657.
13. J. X. Lin, S. L. Zhan, M. H. Fang, X. Q. Qian, and H Yang, *J. Environ. Manage.*, **2008**, 87, 193.
14. M. A. Al-Ghouti, M. A. M. Khraisheh, S. J. Allen, and M. N. Ahmad, *J. Environ. Manage.*, **2003**, 69, 229.
15. R. C. Plaza, F González-Caballero, and A. V. Delgado, *Colloid Polym. Sci.*, **2001**, 279, 1206.
16. S Hong, C Wen, J He, F Gan, and Y.-S. Ho, *J. Hazard. Mater.*, **2009**, 167, 630.
17. C Li, Y Dong, J Yang, Y Li, and C Huang, *J. Mol. Liq.*, **2014**, 196, 348.
18. A. M. Aljeboree, A. N. Alshirifi, and A. F. Alkaim, *Arabian Journal of Chemistry*, **2017**, 10, S3381.
19. R Elmoubarki, *Water Resour. Ind.*, **2015**, 9, 16.
20. Y.-S. Ho, W.-T. Chiu, and C.-C. Wang, *Bioresour. Technol.*, **2005**, 96, 1285.
21. M. A. Rauf, S. M. Qadri, S Ashraf, and K. M. Al-Mansoori, *Chem. Eng. J.*, **2009**, 150, 90.
22. C Jiang, L Jia, B Zhang, Y He, and G Kirumba, *J. Environ. Sci.*, **2014**, 26, 466.
23. M. T. Yagub, T. K. Sen, S Afroze, and H. M. Ang, *Adv. Colloid Interface Sci.*, **2014**, 209, 172.
24. N Dizge, C Aydinler, E Demirbas, M Kobya, and S Kara, *J. Hazard. Mater.*, **2008**, 150, 737.
25. O. A. Attallah, *RSC Adv.*, **2016**, 6, 11461.
26. D Tsiourvas, A Tsetsekou, M Arkas, S Diplas, and E Mastrogianni, *J. Mater. Sci. Mater. Med.*, **2011**, 22, 85.
27. A. M. Bobrova, I. G. Zhigun, M. I. Bragina, and A. A. Fotiev, *J. Appl. Spectrosc.*, **1968**, 8, 59.
28. L. H. Velazquez-Jimenez, R. H. Hurt, J. Matos, and J. R. Rangel-Mendez, *Environ. Sci. Technol.*, **2014**, 48, 1166.
29. A Bera, T Kumar, K Ojha, and A Mandal, *Appl. Surf. Sci.*, **2013**, 284, 87.
30. M Ma, Y Zhang, W. Yu, H Shen, H Zhang, and N Gu, *Colloids Surfaces A Physicochem. Eng. Asp.*, **2003**, 212, 219.
31. D Sun, X Zhang, Y Wu, and X Liu, *J. Hazard. Mater.*, **2010**, 181, 335.
32. C Varlikli, *J. Hazard. Mater.*, **2009**, 170, 27.
33. J. M. Gómez, J Galán, A Rodríguez, and G. M. Walker, *J. Environ. Manage.*, **2014**, 146, 355.
34. F Ferrero, *J. Environ. Sci.*, **2010**, 22, 467.
35. R Lafi, S Rezma, and A Hafiane, *Desalin. Water Treat.*, **2015**, 56, 2754.
36. T. G. M. van de Ven, K Saint-Cyr, and M Allix, *Colloids Surfaces A Physicochem. Eng. Asp.*, **2007**, 294, 1.
37. P Monash and G Pugazhenthii, *Adsorption*, **2009**, 15, 390.
38. C. H. Giles, A. P. D'Silva, and I. A. Easton, *J. Colloid Interface Sci.*, **1974**, 47, 766.
39. V. S. Mane and P. V. V. Babu, *Desalination*, **2011**, 273, 321.
40. R. Y. Talman and G. Atun, *Colloids Surfaces A Physicochem. Eng. Asp.*, **2006**, 281, 15.
41. S. Hamidzadeh, M Torabbeigi, and S. J. Shahtaheri, *J. Environ. Heal. Sci. Eng.*, 2015, 13, 8.
42. O. S. Amodu, T. V. Ojumu, S. K. Ntwampe, and O. S. Ayanda, *J. Encapsulation Adsorpt. Sci.*, **2015**, 5, 191.
43. I Safarik, K Horská, and M Safariková, *J. Cereal Sci.*, **2011**, 53, 78.
44. A Mittal, J Mittal, A Malviya, D Kaur, and V. K. Gupta, *J. Colloid Interface Sci.*, **2010**, 343, 463.
45. M. A. Gabal, E. A. Al-Harthy, Y. M. Al Angari, and M. Abdel Salam, *Chem. Eng. J.*, 2014, 255, 156.
46. M Alshabanat, G Alsenani, and R Almufarij, *J. Chem.*, **2013**, 2013, 1.
47. G ANNADURAI, R JUANG, and D LEE, *J. Hazard. Mater.*, **2002**, 92, 263.
48. T Zehra, N Priyantha, and L. B. L. Lim, *Environ. Earth Sci.*, **2016**, 75, 357.
49. C.-C. Kan, M. C. Aganon, C. M. Futralan, and M. L. P. Dalida, *J. Environ. Sci.*, **2013**, 25, 1483.
50. R Kumar and R Ahmad, *Desalination*, **2011**, 265, 112.